

# Kv4.2 mRNA Abundance and A-Type K<sup>+</sup> Current Amplitude Are Linearly Related in Basal Ganglia and Basal Forebrain Neurons

Tatiana Tkatch, Gytis Baranauskas, and D. James Surmeier

Department of Physiology and Institute for Neuroscience, Northwestern University Medical School, Chicago, Illinois 60611

A-type K<sup>+</sup> currents are key determinants of repetitive activity and synaptic integration. Although several gene families have been shown to code for A-type channel subunits, recent studies have suggested that Kv4 family channels are the principal contributors to A-type channels in the somatodendritic membrane of mammalian brain neurons. If this hypothesis is correct, there should be a strong correlation between Kv4 family mRNA and A-type channel protein or aggregate channel currents. To test this hypothesis, quantitative single-cell reverse transcription-PCR analysis of Kv4 family mRNA was combined with voltage-clamp analysis of A-type K<sup>+</sup> currents in acutely isolated neurons. These studies revealed that Kv4.2 mRNA abundance was linearly related to A-type K<sup>+</sup> current amplitude in neostriatal medium spiny neurons and cholinergic

interneurons, in globus pallidus neurons, and in basal forebrain cholinergic neurons. In contrast, there was not a significant correlation between estimates of Kv4.1 or Kv4.3 mRNA abundance and A-type K<sup>+</sup> current amplitudes. These results argue that Kv4.2 subunits are major constituents of somatodendritic A-type K<sup>+</sup> channels in these four types of neuron. In spite of this common structural feature, there were significant differences in the voltage dependence and kinetics of A-type currents in the cell types studied, suggesting that other determinants may create important functional differences between A-type K<sup>+</sup> currents.

**Key words:** Kv4; A-type K<sup>+</sup> channel; voltage clamp; single-cell RT-PCR; TEA; 4-AP; potassium channels; mRNA

Voltage-dependent K<sup>+</sup> channels regulate virtually every aspect of the electrophysiological behavior of neurons. K<sup>+</sup> channels govern processes as diverse as subthreshold synaptic integration, spike repolarization, and repetitive spiking. To fill these functional niches, a broad array of K<sup>+</sup> channels has evolved, each with biophysical properties tailored to their role in cellular behavior (Hille, 1992). One of the first examples of this kind of tailoring was found in invertebrate neurons where an unusual K<sup>+</sup> current enabled slow repetitive spiking (Hagiwara et al., 1961; Connor and Stevens, 1971). In the last 20 years, rapidly inactivating, A-type K<sup>+</sup> currents have been found in a wide variety of mammalian neurons (Rudy, 1988). However, the biophysical properties of A-type currents have often diverged significantly from those found initially in invertebrate neurons. For example, some A-type (or “A-like”) currents inactivate rapidly but recover from inactivation very slowly, taking seconds at hyperpolarized membrane potentials. Other A-type currents activate only at suprathreshold membrane potentials, rather than at subthreshold potentials, predisposing them to a role in spike repolarization. This biophysical diversity is matched by the molecular heterogeneity of A-type channels revealed by molecular cloning. At least six genes code for K<sup>+</sup> channel subunits that form A-type channels in heterologous expression systems: Kv1.4, Kv3.4, Kv4.1–3, and erg3 (Stuhmer et al., 1989; Baldwin et al., 1991; Pak et al., 1991; Roberds and Tamkun, 1991; Schroter et al., 1991; Serodio et al.,

1996; Shi et al., 1997). The molecular picture is further complicated by the ability of auxiliary channel subunits to transform non-inactivating, delayed rectifier K<sup>+</sup> channels into inactivating, A-type channels (Rettig et al., 1994; Heinemann et al., 1996). In spite of this complexity, only channels composed of Kv4 family subunits appear to have properties similar to those originally described in invertebrates—that is, an ability to open at subthreshold membrane potentials and to recover quickly from inactivation (Serodio et al., 1994).

A-type K<sup>+</sup> channels with Kv4-like properties are prominent in the somatodendritic membrane of many mammalian brain neurons, including neurons in the basal ganglia. In some of these neurons, there is strong evidence that A-type K<sup>+</sup> channels are composed of Kv4 family subunits. For example, single-cell reverse transcription-PCR (scRT-PCR) and patch-clamp studies have shown that A-type K<sup>+</sup> currents in neostriatal cholinergic neurons are attributable to K<sup>+</sup> channels containing Kv4.2  $\alpha$  subunits (Song et al., 1998). Other studies using similar strategies have been able to provide compelling evidence of functional Kv4 family channels in somatodendritic regions of other central and peripheral neurons (Johns et al., 1997; Dryer et al., 1998; Martina et al., 1998). Immunocytochemical studies are also consistent with this picture (Sheng et al., 1992; Maletic-Savatic et al., 1995; Alonso and Widmer, 1997). What is not clear from these studies is the extent to which the low-threshold, rapidly recovering A-type current is solely attributable to channels composed of Kv4 family subunits. A determination of the molecular architecture of the A-type channels in these neurons not only has fundamental implications for our understanding of their computational properties and modulation but is essential to transgenic strategies aimed at normalizing aberrant activity patterns found in psychomotor diseases of the basal ganglia, like Parkinson's disease.

Received Aug. 26, 1999; revised Oct. 15, 1999; accepted Oct. 22, 1999.

This work was supported by the National Institutes of Health National Institute of Neurological Disorders and Stroke Grants NS 34696 and NS 26473 to D.J.S. We also thank Dr. Teepu Siddique for his help in some of these experiments.

Correspondence should be addressed to Dr. D. James Surmeier, Department of Physiology/Northwestern University Institute for Neuroscience, Northwestern University Medical School, 320 East Superior Street, Chicago, IL 60611. E-mail: j-surmeier@nwu.edu.

Copyright © 2000 Society for Neuroscience 0270-6474/00/200579-10\$15.00/0

## MATERIALS AND METHODS

**Tissue preparation.** Globus pallidus, neostriatal, and basal forebrain neurons from young adult rats (4–6 weeks postnatal) were dissociated acutely, using procedures similar to those we have described previously (Surmeier et al., 1995). In brief, rats were anesthetized with methoxyflurane and decapitated; brains were quickly removed, iced, and blocked for slicing. Sagittal slices (350  $\mu$ m) were cut with a Microslicer (Dosaka, Kyoto, Japan) while bathed in 0  $\text{Ca}^{2+}$  solution containing (in mM): 140 sodium isethionate, 2 KCl, 4  $\text{MgCl}_2$ , 23 glucose, and 15 HEPES, pH 7.4 (300–305 mOsm/l). Slices were incubated for 1–6 hr at room temperature (20–22°C) in  $\text{NaHCO}_3$ -buffered saline bubbled with 95%  $\text{O}_2$  and 5%  $\text{CO}_2$  containing (in mM): 126 NaCl, 2.5 KCl, 2  $\text{CaCl}_2$ , 2  $\text{MgCl}_2$ , 26  $\text{NaHCO}_3$ , 1.25  $\text{NaH}_2\text{PO}_4$ , 1 pyruvic acid, 0.2 ascorbic acid, 0.1  $N^G$ -nitro-L-arginine, 1 kynurenic acid, and 10 glucose, pH 7.4 (300–305 mOsm/l). Slices were then removed into the 0  $\text{Ca}^{2+}$  solution, and regions of globus pallidus or dorsal neostriatum were dissected with the aid of a dissecting microscope. Dissected tissue was placed in an oxygenated Cell-Stir chamber (Wheaton, Millville, NJ) containing pronase (Sigma protease type XIV; 1–2 mg/ml; St. Louis, MO) in HEPES-buffered HBSS (Sigma) at 35°C. After 20–40 min of enzyme digestion, the tissue was rinsed three times in 0  $\text{Ca}^{2+}$  buffer and dissociated mechanically with a graded series of fire-polished Pasteur pipettes. The cell suspension was then plated into a 35 mm Lux Petri dish containing HEPES-buffered HBSS saline. The dish was then placed on the stage of an inverted microscope. All reagents were obtained from Sigma.

**Electrophysiological methods.** Whole-cell recordings used standard techniques (Hamill et al., 1981; Song et al., 1998). Electrodes were pulled from Corning (Corning, NY) 7052 glass and fire-polished before use. The electrode solution consisted of (in mM): 30–60  $\text{K}_2\text{SO}_4$ , 30–60  $N$ -methyl- $D$ -glucamine, 2  $\text{MgCl}_2$ , 40 HEPES, 5 EGTA, 12 phosphocreatine, 2  $\text{Na}_2\text{ATP}$ , 0.2  $\text{Na}_2\text{GTP}$ , and 0.1 leupeptin, pH 7.2 with  $\text{H}_2\text{SO}_4$  (osmolality, 260–270 mOsm/l). The external solution consisted of (in mM): 140 sodium isethionate, 2 KCl, 4  $\text{MgCl}_2$ , 10 HEPES, 12 glucose, and 0.001 TTX, pH 7.35 with NaOH (osmolality, 295–305 mOsm/l).

In all experiments,  $\text{Na}^+$  currents were blocked with TTX, and  $\text{Ca}^{2+}$  currents were eliminated by replacing calcium with magnesium in the external solution. In some experiments, 4-aminopyridine (4-AP; Sigma) or tetraethylammonium chloride (TEA; Sigma) was applied. When 4-AP was included in the extracellular solutions, the pH was adjusted to 7.35 using  $\text{H}_2\text{SO}_4$ . When 4-AP and TEA were applied at concentrations >1 mM, the osmolality was adjusted by reducing the concentration of sodium isethionate. Solutions were applied by a gravity-fed sewer pipe system. An array of application capillaries (~400  $\mu$ m in inner diameter) was positioned a few hundred micrometers from the cell under study. Solution changes were made by altering the position of the array with a DC drive system and microprocessor-based controller (Newport, Irvine, CA). Solution changes were complete within <1 sec.

Recordings were obtained with an Axon Instruments 200 patch-clamp amplifier and interface that was controlled and monitored with a personal computer running pCLAMP software (version 7.0; Axon Instruments, Foster City, CA). Electrode resistance was typically 1.5–2.2 M $\Omega$  in the bath. After seal rupture, series resistance (4–10 M $\Omega$ ) was compensated (75–90%) and periodically monitored. Potentials were not corrected for the liquid junction potential, which was estimated to be 1–2 mV. All averaged data presented as the mean  $\pm$  SEM. Fits to the data were obtained using Igor Pro (version 3.12; WaveMetrics, Lake Oswego, OR). Activation data were fit with a Boltzmann equation of the form:  $1/(1 + \exp((V - V_h)/V_c))$ , where  $V$  stands for membrane potential,  $V_h$  stands for the half-activation voltage, and  $V_c$  is the slope factor. Maximum conductance estimates were generated by (1) fitting the inactivation phase of A-type current evoked by a step to 0 mV (from a holding potential of –120 mV) with an exponential function, (2) extrapolating back to the initiation of the evoking step, and (3) dividing by the  $\text{K}^+$ -driving force. This value was then corrected to account for incomplete activation using parameters derived from the steady-state activation plots (see Fig. 2). Dose–response data were fit with a Langmuir isotherm of the form:  $C/(C + \text{IC}_{50})^n$ , where  $C$  stands for a concentration of the blocking agent,  $\text{IC}_{50}$  has the usual meaning, and  $n$  is the cooperativity factor that was routinely set to 1.

**scRT-PCR methods.** Neurons were harvested for scRT-PCR profiling in one of two ways. To maximize mRNA yields, some neurons were aspirated without recording. Isolated neurons were patched in the cell-attached mode and lifted into a stream of control solution. Neurons were then aspirated into the electrode. Electrodes contained ~5  $\mu$ l of sterile water. In other experiments, neurons were subjected to whole-cell

voltage-clamp recordings before aspiration. In these cases, the electrode recording solution was made nominally RNase-free, and the total volume was kept near 5  $\mu$ l. In both sets of experiment, the capillary glass used for making electrodes was heated to 200°C for 1 hr. Sterile gloves were worn during the procedure to minimize RNase contamination. After aspiration of the neuron, the electrode was removed from the holder, the tip was broken in a 0.5 ml Eppendorf tube containing 3.6  $\mu$ l of diethylpyrocarbonate-treated water, 0.7  $\mu$ l of RNasin (28,000 U/ml), and 0.7  $\mu$ l of oligo-dT (0.5  $\mu\text{g}/\mu\text{l}$ ), and the contents were ejected. The mixture was heated to 70°C and then placed on ice for 1 min. Single-strand cDNA was synthesized from the cellular mRNA by adding SuperScript II RT (1  $\mu$ l; 200 U/ $\mu$ l), 10 $\times$  PCR buffer,  $\text{MgCl}_2$  (2  $\mu$ l; 25 mM), DTT (2  $\mu$ l; 0.1 M), and mixed dNTPs (1  $\mu$ l; 10 mM) and then incubating the mixture at 42°C for 50 min. The reaction was terminated by heating the mixture to 70°C for 15 min. The RNA strand in the RNA–DNA hybrid was then removed by adding 1  $\mu$ l of RNase H (2 U/ $\mu$ l) and incubating at 37°C for 20 min. All reagents except RNasin (Promega, Madison, WI) were obtained from Life Technologies (Grand Island, NY). Preliminary experiments revealed that the efficiency of reverse transcription could vary by more than a factor of two in different enzyme lots. Therefore, all of the quantitative experiments presented here were done with the same enzyme lot.

The single-cell cDNA generated from the reverse transcription step was subjected to conventional PCR using a programmable thermal cycler (MJ Research, Watertown, MA). PCR primers were developed from GenBank sequences with commercially available OLIGO software (National Biosciences, Plymouth, MN). Primers for choline acetyltransferase (ChAT), the 67 kDa isoform of glutamate decarboxylase (GAD67), substance P, enkephalin, Kv3.4, and Kv4.1–3 have been described previously (Surmeier et al., 1996; Song et al., 1998; Tkatch et al., 1998). PCR procedures were performed using procedures designed to minimize the chance of cross-contamination (Cimino et al., 1990). Negative controls for contamination from extraneous and genomic DNA were run for every batch of neurons. To ensure that genomic DNA did not contribute to the PCR products, neurons were aspirated and processed in the normal manner, except that the reverse transcriptase was omitted. Contamination from extraneous sources was checked by replacing the cellular template with water. Both controls were consistently negative in these experiments.

To calibrate the Kv4.2 amplification, a cDNA standard was generated. To do this, a Kv4.2 cDNA fragment was obtained by amplification of whole-brain cDNA. The primer set was designed to generate a cDNA that spanned the region targeted by the previously described Kv4.2 primer set (Song et al., 1998). The upper primer was 5'-AAC CGG CCT TCG TTA GCA AA (position 1939), and the lower primer was 5'-TTC GGA CCA AGA AGT CAC CTA AAA C (position 2634). The cDNA fragment was cloned in the pGEM-T vector (Promega) according to the manufacturer's instructions. The sequence identity was verified by automated sequencing performed at the Northwestern University Biotechnology laboratory. Plasmid was linearized by *SalI* digestion, and its concentration was determined using Kodak image analysis software (Eastman Kodak, Rochester, NY) by comparison with DNA of known concentration.

Quantitative analysis of Kv4.2 cDNA abundance was performed on the ABI PRISM 7700 Sequence Detector System (Perkin-Elmer, Foster City, CA). The following pair of primers was used: 5'-CGT GAC CAC AGC AAT AAT TAG CA (position 2327) and 5'-TTC CTC CCG AAT ACT CAG GAG ACT (position 2335). Real-time detection of PCR amplicons was accomplished with a fluorescent TaqMan probe whose sequence was TCC AAC ACC TCC AGT AAC CAC CCC A. Four microliters of cellular cDNA (one-fifth of the total) were used as a template in 50  $\mu$ l of buffer solution. The reaction was performed according to the manufacturer's instructions. A calibration curve was obtained by amplification of Kv4.2 plasmid DNA with single-strand copy numbers ranging from 1 to 200. Template controls were included in each run.

## RESULTS

### Neostriatal, pallidal, and basal forebrain neurons express A-type $\text{K}^+$ currents

For the purposes of comparison, four types of telencephalic neuron were examined in this study: neostriatal medium spiny neurons (MS), neostriatal cholinergic interneurons (ChAT/str), globus pallidus neurons (GP), and basal forebrain cholinergic

neurons (ChAT/bf). Neurons were dissociated from the appropriate brain region and then subjected to patch-clamp recording. Neurons were unequivocally identified after recording by scRT-PCR analysis of phenotyping mRNAs (Song and Surmeier, 1996; Tkatch et al., 1998). MS neurons were identified by their expression of substance P and/or enkephalin mRNA. ChAT/str and ChAT/bf neurons were identified by their expression of ChAT mRNA. GP neurons were identified by their expression of GAD67 and the absence of ChAT mRNA (Tkatch et al., 1998).

Previous work has demonstrated that all four cell types express a low-threshold A-type  $K^+$  current that is relatively insensitive to TEA (Surmeier et al., 1989; Stefani et al., 1992; Sim and Allen, 1998; Song et al., 1998). To verify these results in our sample, acutely isolated neurons were subjected to voltage-clamp analysis.  $K^+$  currents were isolated pharmacologically and evoked by stepping the membrane potential to  $-30$  mV, a potential that should effectively activate low-threshold currents but not delayed rectifiers. In addition to their activation voltage dependence, a hallmark of A-type  $K^+$  currents is their rapid inactivation at depolarized membrane potentials (Connor and Stevens, 1971). This feature has been used in a number of studies to isolate A-type  $K^+$  currents. This strategy was partially successful in the neurons studied here. The  $K^+$  currents evoked after hyperpolarized ( $-95$  mV) and depolarized ( $-45$  mV) conditioning steps (100 msec) are shown in the *left column* of Figure 1. As expected, in most neurons the currents evoked from  $-95$  mV had a transient, rapidly inactivating component, whereas the currents evoked from  $-45$  mV did not. By subtracting these traces, an inactivating, A-type current could be isolated, as shown in the *right column* of Figure 1 (difference currents). However, in GP neurons this strategy was not very effective in isolating a current with the expected features (Fig. 1, *bottom right*).

Another hallmark of the Kv4 family A-type  $K^+$  current is its relative insensitivity to TEA. To provide a more complete isolation, difference currents were measured with 20 mM TEA in the bath. In neostriatal cholinergic interneurons (Fig. 1, *top*), TEA had a marginal effect on the difference currents. Slowly inactivating currents were clearly reduced in the other cell types, however. The improvement in the isolation afforded by TEA was particularly prominent for GP neurons (Fig. 1, *bottom*). As a consequence, with the exception of work with neostriatal cholinergic interneurons, subsequent experiments were performed in the presence of 20–50 mM TEA.

### Activation properties of A-type currents

As is evident in the records in Figure 1, there were substantial differences in the kinetics of the currents isolated by this regimen. As a consequence, a more complete biophysical study of A-type currents was undertaken. To characterize activation properties, A-type currents were isolated as shown in Figure 2*A* (a strategy similar to that shown in Fig. 1). Activation time constants ( $\tau_{act}$ ) were obtained by fitting traces with a single exponential. The results are summarized in Figure 2*B*. A-type currents in ChAT/str ( $n = 4$ ) and MS ( $n = 5$ ) neurons displayed little voltage dependence and had time constants that were very similar. On the other hand, A-type currents in GP ( $n = 4$ ) and ChAT/bf ( $n = 4$ ) neurons activated more slowly at membrane potentials near threshold, and activation time constants decreased significantly with progressive depolarization.

Steady-state activation voltage dependence was also determined for each cell type. A plot of mean normalized peak chord conductance as a function of test pulse voltage is shown in Figure

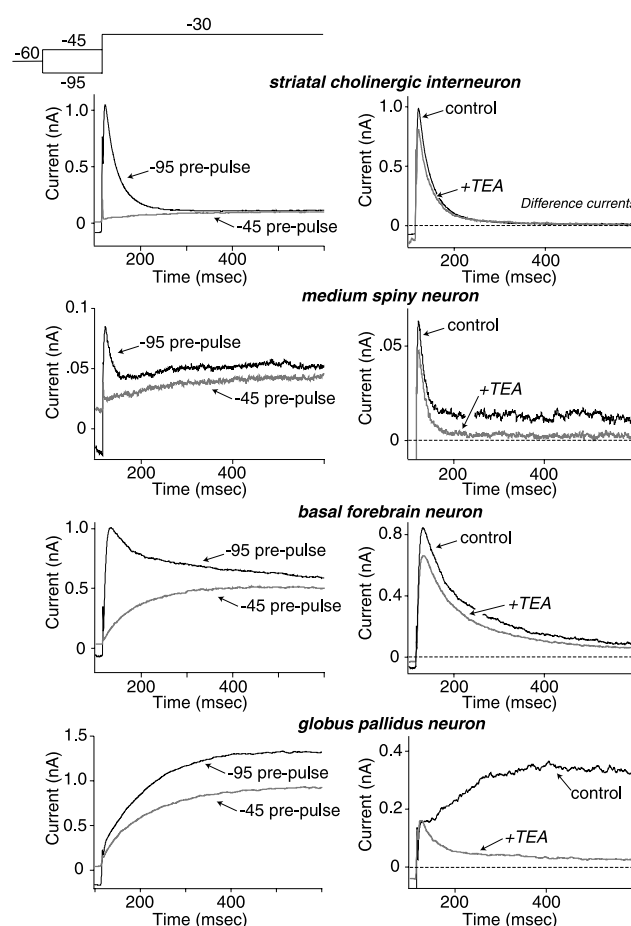


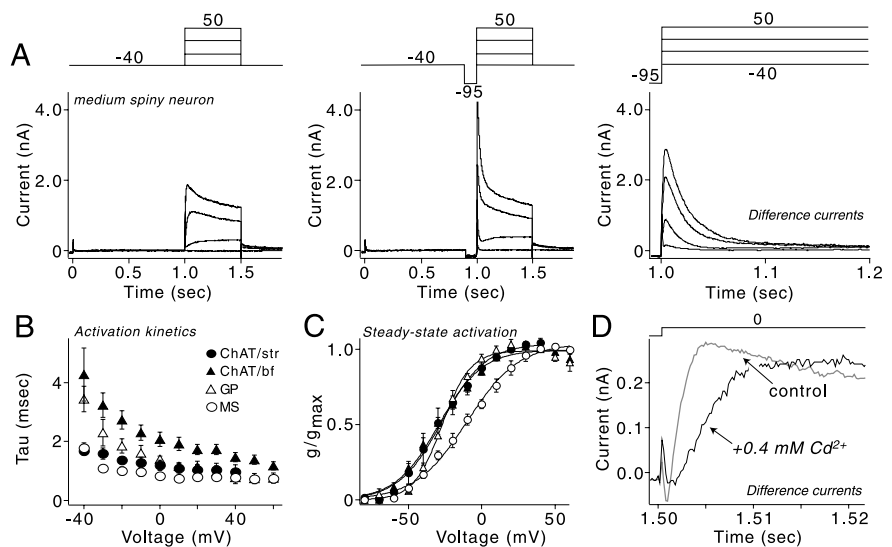
**Figure 1.** Low-threshold, TEA-resistant A-type current was present in most of the neurons tested. *Left Column*, Current traces evoked by the voltage-clamp protocol shown on the top in each of the cell types studied are shown. *Right Column*, The difference currents from the column on the left are shown (control). In addition, the difference currents recorded in the presence of 20–50 mM TEA are shown. Note the improved isolation afforded by the addition of TEA.

2*C*. The data from each cell type were well fit with Boltzmann function. In both ChAT/str ( $n = 4$ ) and ChAT/bf ( $n = 4$ ) neurons, these fits were virtually identical ( $V_h = -27$  and  $-29$  mV, respectively, and  $V_c = 14.8$  mV for both cell types). In GP neurons ( $n = 4$ ), the voltage dependence of activation was steeper ( $V_c = 9.6$  mV;  $V_h = -27$  mV), whereas in MS neurons ( $n = 5$ ), it was shallower ( $V_c = 17.7$  mV). Last, in MS neurons, A-type current activated at more positive potentials ( $V_h = -10$  mV) than in the remaining three cell types. In agreement with the pooled data, statistical analysis of the half-activation voltages in individual neurons showed that although ChAT/str, ChAT/bf, and GP neurons were indistinguishable ( $p > 0.05$ , Kruskal–Wallis), MS neurons activated at significantly more depolarized potentials ( $p < 0.05$ , Kruskal–Wallis).

Another feature that distinguishes Kv4 family channels is their allosteric regulation by divalent cations like  $Cd^{2+}$  (Fiset et al., 1997; Wickenden et al., 1999). In cholinergic interneurons, 200  $\mu M$   $Cd^{2+}$  shifts the voltage dependence of Kv4.2 channel gating by  $>20$  mV (Song et al., 1998). Qualitatively similar results were obtained for all three of the other cell types (data not shown). In addition,  $Cd^{2+}$  slowed activation kinetics by more than would be predicted solely on the basis of the change in activation voltage



**Figure 2.** A-type currents differed in voltage dependence and kinetics of activation in the four cell types. **A**, Currents evoked by depolarizing steps ( $-30$  to  $+30$  mV) after a prepulse (1 sec) to  $-40$  mV (left) were subtracted from those evoked by a similar protocol except that a brief (100 msec) prepulse to  $-95$  mV was added immediately before the test steps (middle). Difference currents are shown on the right. Neurons were recorded in the presence of 50 mM TEA. **B**, Activation time constants obtained by fitting the rising phase of the difference currents are shown. Average time constants are plotted as a function of the test pulse voltage for the four cell types. Filled triangles, ChAT/bf neurons ( $n = 4$ ); open triangles, GP neurons ( $n = 4$ ); filled circles, ChAT/str neurons ( $n = 4$ ); and open circles, MS cells ( $n = 5$ ). **C**, Plot of the average peak conductance as a function of test pulse voltage for the four cell types is shown. Filled triangles, ChAT/bf neurons ( $n = 4$ ); open triangles, GP neurons ( $n = 4$ ); filled circles, ChAT/str neurons ( $n = 4$ ); and open circles, MS cells ( $n = 5$ ). Boltzmann fits were obtained for each cell type. **D**, Application of 0.4 mM  $\text{Cd}^{2+}$  dramatically reduced the activation rate of A-type current in an MS neuron. Difference currents generated by a step to 0 mV from  $-95$  and  $-45$  mV prepulses are shown.



dependence. For example, in medium spiny neurons there was only a small acceleration in activation kinetics with increasing depolarization (Fig. 2*B*), but the activation time constant at 0 mV was slowed by a factor of approximately three by  $\text{Cd}^{2+}$  (Fig. 2*D*).

### Inactivation properties of A-type currents

The steady-state voltage dependence of inactivation was studied by stepping to membrane potentials between  $-45$  and  $-120$  mV for 1.5 sec before a test step to 0 mV. An example of the currents generated by this protocol in a globus pallidus neuron is shown in Figure 3*A*. A plot of mean normalized peak currents as a function of conditioning voltage for each cell type is shown in Figure 3*B*. In each case, the data were well fit with a Boltzmann function. In both ChAT/str ( $n = 6$ ) and ChAT/bf ( $n = 6$ ) neurons, the voltage dependence of inactivation was virtually identical ( $V_h = -93$  mV in ChAT/str neurons and  $-91.7$  mV in ChAT/bf neurons). In GP ( $n = 6$ ) and MS ( $n = 5$ ) neurons, the inactivation voltage dependence was progressively more depolarized ( $V_h = -82.8$  mV in GP neurons and  $-75.6$  mV in MS neurons). In agreement with the pooled data, statistical analysis of half-inactivation voltages in individual neurons revealed no differences between ChAT-expressing cell types ( $p > 0.05$ , Kruskal–Wallis) but that both GP and MS neurons inactivated at significantly more depolarized potentials ( $p < 0.05$ , Kruskal–Wallis). The half-inactivation voltages of MS and GP neurons were not significantly different ( $p > 0.05$ , Kruskal–Wallis).

One of the features that differentiated the A-type currents shown in Figure 1 was inactivation rate. To generate a more systematic picture of how the kinetics differed, the decay of current at 0 mV was fit with single or double exponential functions. In MS neurons ( $n = 5$ ), the inactivation was fast ( $\sim 10$ – $15$  msec time constant) and primarily monoexponential (Fig. 3*C*). The inactivation of A-type current in ChAT/str neurons ( $n = 6$ ) was also typically monoexponential (Fig. 3*C*), although slower than that in MS neurons ( $p < 0.05$ , Kruskal–Wallis). In contrast, in all ChAT/bf ( $n = 6$ ) and in most GP ( $n = 6$ ) cells, the inactivation process was clearly biexponential. In these cells, the fast time constant was similar to that found in ChAT/str neurons (see Fig. 3*C*, insets). The slower time constant was  $100$ – $200$  msec and comprised  $55 \pm 3\%$  of the total current in ChAT/bf neurons

and  $61 \pm 6\%$  in GP neurons (in three of the seven GP neurons, the slower component accounted for all of the inactivation).

Rapid recovery from inactivation is a key feature of A-type currents regulating repetitive discharge and synaptic input (Connor and Stevens, 1971; Kanold and Manis, 1999). This feature also distinguishes Kv1.4 and Kv4 family channels (Bertoli et al., 1994, 1996; Serodio et al., 1994; Petersen and Nerbonne, 1999). As a consequence, recovery kinetics was examined in each cell type. As shown in Figure 4*A*, A-type currents were inactivated by holding the cell at  $-40$  mV, and then recovery was produced by stepping to  $-95$  mV for varying periods of time before a test step to 0 mV. In MS neurons, it was necessary to subtract slowly inactivating currents; these were isolated using the same protocol with an added brief (50 msec) step to 0 mV just before the test step (data not shown). Examples of peak current recovery as a function of prepulse duration are shown in Figure 4*D*. In most neurons, the recovery process was biexponential. The fast recovery time constant varied from  $8.7 \pm 1.2$  msec in MS neurons ( $n = 6$ ) to  $62 \pm 14$  msec in GP cells ( $n = 11$ ); the fast time constant of recovery was  $30 \pm 3$  msec ( $n = 11$ ) in ChAT/str neurons and  $57 \pm 10$  msec ( $n = 4$ ) in ChAT/bf neurons. The slow recovery time constant varied somewhat less [ $109 \pm 15$  msec in MS cells;  $297 \pm 64$  msec in ChAT/bf neurons ( $n = 4$ );  $363 \pm 74$  msec in GP cells; and  $477 \pm 42$  msec in ChAT/str neurons ( $n = 11$ )]. One of the biggest differences among the cell types was the percentage of the current that recovered rapidly. In MS neurons, for example, the rapidly recovering component comprised  $75 \pm 4\%$  of the total current. In contrast, a rapidly recovering component was completely absent in some GP neurons (3 of 11). In ChAT/str and ChAT/bf neurons, the rapidly recovering component of the current was of intermediate amplitude ( $44 \pm 4$  and  $38 \pm 4\%$ , respectively).

### Serial dilution experiments show that Kv4.2 mRNA abundance is related to A-type current amplitude

Initially, Kv4 family mRNA expression was characterized using conventional scRT-PCR approaches aimed at transcript detection (Audinot et al., 1996; Surmeier et al., 1996; Yan and Surmeier, 1996). These experiments showed that neurons in each group had detectable levels of Kv4 family mRNAs (data not shown). How-

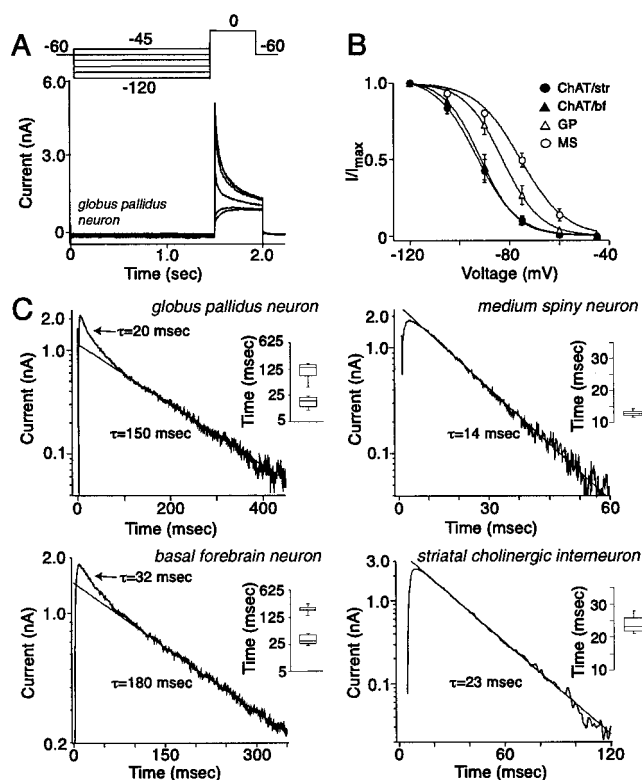


**Figure 3.** A-type currents differed in inactivation voltage dependence and kinetics. *A*, Conditioning pulses (1.5 sec long) were used to test the voltage dependence of inactivation. *B*, Plot of peak current amplitude versus voltage of the conditioning prepulse is shown. Filled triangles, ChAT/bf neurons ( $n = 6$ ); open triangles, GP neurons ( $n = 6$ ); filled circles, ChAT/str neurons ( $n = 6$ ); and open circles, MS cells ( $n = 5$ ). Thin lines show Boltzmann fits. *C*, Semilogarithmic plots of current traces show that the development of inactivation could be fit by a biexponential function in GP and ChAT/bf neurons and by a monoexponential function in MS and ChAT/str cells. Thin straight lines represent monoexponential fits. Insets, Box plot summaries of rate constants for each cell type are shown: ChAT/bf neurons ( $n = 6$ ), GP neurons ( $n = 6$ ), ChAT/str neurons ( $n = 6$ ), and MS cells ( $n = 5$ ).

ever, not every transcript was detected in every neuron. Detection frequencies  $<100\%$  can be interpreted in one of two ways: either (1) there are two or more neuronal subpopulations differing in expression of the targeted transcript or (2) the neuronal population is homogenous but the transcript of interest is of low abundance and near the detection threshold.

To differentiate between these possibilities, semiquantitative scRT-PCR techniques were used. To obtain semiquantitative estimates of mRNA abundance, serial dilution experiments were performed (Sykes et al., 1992; Tkatch et al., 1998). The strategy in these experiments is to determine the smallest fraction of the total cellular cDNA that can be used in the PCR reaction to produce a visually detectable band of the appropriate size in an ethidium bromide-stained gel. The greater the abundance of a particular template, the smaller the fraction of the cellular cDNA that will be required to reach the detection threshold. This allows the relative abundance of a particular mRNA to be determined. Because the same transcripts are examined in different cell types, implicit controls for reverse transcription and PCR efficiency are built into this approach.

Initially, neurons were aspirated without concomitant whole-cell voltage-clamp recording. Cellular mRNA was reverse tran-

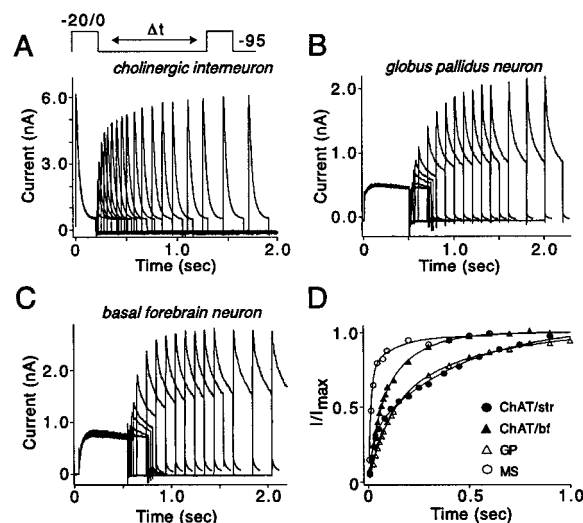


**Figure 4.** Recovery from inactivation varied among cell types. The protocol used is depicted at the top of *A*. In ChAT/str neurons, the test pulse was to  $-20$  mV to reduce current amplitude. In all other cell types, the test pulse was to  $0$  mV. *A–C*, Examples of recovery of A-type current in a ChAT/str neuron (*A*), a globus pallidus neuron (*B*), and a basal forebrain neuron (*C*) are shown. *D*, The normalized peak current is plotted against the duration of conditioning prepulse for the examples shown in *A–C*. In addition, an example from an MS neuron is added. Thin lines show biexponential fits.

scribed, and the resulting cDNA was analyzed for phenotyping transcripts. Identified neurons were then subjected to the serial dilution analysis of Kv4 family mRNAs. Because of our previous work (Song et al., 1998), Kv4.2 transcript abundance was examined first. As shown in Figure 5, there were consistent differences in the abundance of Kv4.2 cDNA in these four neuronal populations. Kv4.2 transcript abundance was the lowest in MS neurons where the amplitude of the A-type currents was smallest. An example of a gel showing the serial dilution of the cDNA from a single MS neuron is shown in Figure 5*A* (left). In this neuron, the detection threshold was one-quarter ( $2^{-2}$ ) of the total cellular cDNA. In Figure 5*A* (right) is a summary of the detection thresholds in our sample of MS neurons. In this case, the distribution of thresholds was not reasonably fit with a single Gaussian but required the sum of two, suggesting that there were two populations of MS neurons. Maximum A-type conductance estimates from identified MS neurons also appeared to be distributed in two groups (see Fig. 5*A*, inset). There was no correlation between the Kv4.2 cDNA detection threshold and the expression of substance P or enkephalin mRNA in MS neurons. GP neurons had a modal detection threshold near one-eighth ( $2^{-3}$ ) of the total cellular cDNA (Fig. 5*B*). As is evident from the distribution of threshold in GP neurons, there also appears to be a subpopulation of GP neurons that has very low or undetectable levels of Kv4.2 mRNA. There was not a clear correlation between this group and the expression of mRNA for another pallidal marker, parvalbumin. Kv4.2 abundance was considerably higher in the cholinergic neurons from the neostriatum and basal forebrain. As shown in Figure 5*C*, the modal detection threshold in ChAT/bf neurons was less than one-sixteenth ( $2^{-4}$ ) of the total cDNA. In ChAT/str neurons, the modal detection threshold was near one-sixty fourth ( $2^{-6}$ ) of the total cDNA (Fig. 5*D*). As indicated in Figure 5, the mean amplitude of A-type currents increased in parallel with the estimated Kv4.2 abundance, with currents being smallest in MS neurons and largest in ChAT/str neurons.

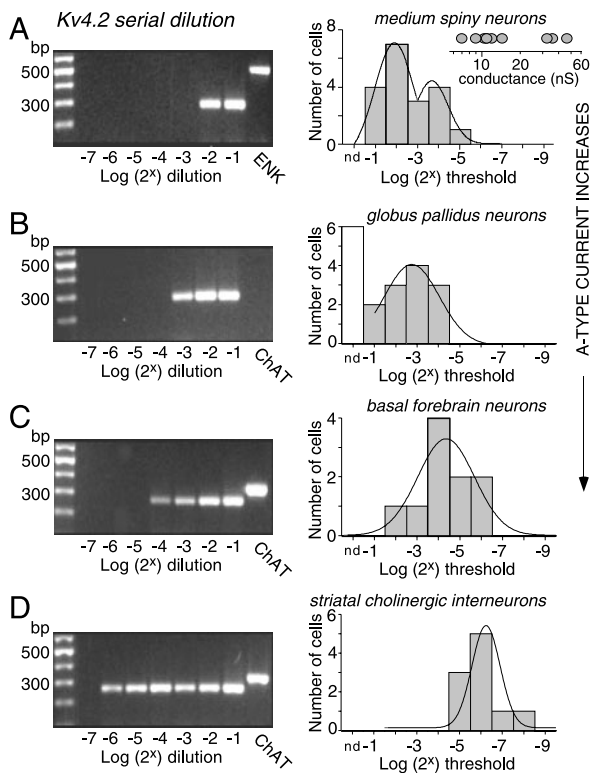


**Figure 5.** Serial dilutions show that Kv4.2 mRNA abundance is correlated with A-type current amplitude. Cell types are arranged from *top to bottom* in increasing mean A-type current amplitude. Representative single-cell serial dilution gels for Kv4.2 cDNA are shown for each cell type in the *left column*. Summary distributions for detection thresholds are shown in the *column on the right*. *A, Left*, A photo of a gel from a typical MS neuron having a detection threshold of one-quarter ( $2^{-2}$ ) of the total cDNA is shown. *Right*, The threshold distribution was best fit with a sum of Gaussian functions (*solid line*). *Inset*, A line plot of maximum conductances in a sample of medium spiny neurons is shown. It revealed a high and low conductance group, in accord with the detection data. *B, Left*, A photo of a gel from a GP neuron in which the detection threshold was one-eighth ( $2^{-3}$ ) of the total cDNA is shown. *Right*, The threshold distribution had a mode near this point, but also note the large number of cells in which the transcript was not detected (*nd*; see *open bar*). *C, Left*, A photo of a gel from a typical basal forebrain neuron having a detection threshold of one-sixteenth ( $2^{-4}$ ) of the total cDNA is shown. *Right*, The threshold distribution was best fit with a single Gaussian function (*solid line*) with a mode near the same dilution. *D, Left*, A photo of a gel from a typical neostriatal cholinergic neuron having a detection threshold of one-sixty fourth ( $2^{-6}$ ) of the total cDNA is shown. *Right*, The threshold distribution was best fit with a single Gaussian function (*solid line*) with a mode near the same dilution. In each gel, the *left-hand lane* is a sizing ladder. The *right-hand lane* is for phenotyping cDNAs enkephalin (*ENK*) and ChAT. The *seven lanes* in between are PCR products obtained after using an increasing (from *left to right*) amount of total cellular cDNA (as denoted *below*) to detect Kv4.2 cDNA.

In contrast, there was little or no correlation between A-type current amplitude and estimates of Kv4.1 or Kv4.3 abundance. Shown in Figure 6 are the threshold distributions for Kv4.1 and Kv4.3 transcripts in each of the four sampled populations. Again, the populations are ordered from *top to bottom* in increasing mean amplitude of A-type currents. Kv4.1 mRNA levels were similar in all four cells (Fig. 6, *left*). ChAT/bf neurons displayed the highest abundance where the modal detection threshold was one-eighth of the total cellular cDNA (approximately three times lower than that in GP cells). In the remaining three cell types, Kv4.1 abundance differed by less than a factor of two. In contrast,

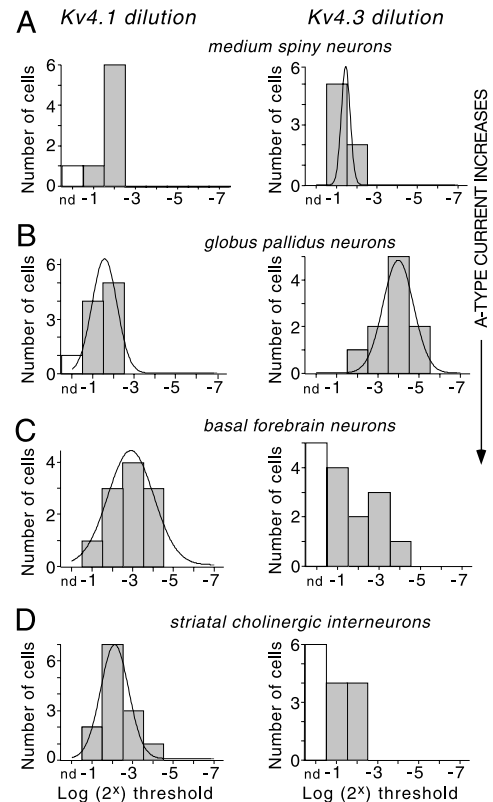


**Figure 6.** Serial dilutions show that Kv4.1 and Kv4.3 mRNA abundance is not correlated with A-type current amplitude. Cell types are arranged from *top to bottom* in increasing mean A-type current amplitude. Summary distributions for detection thresholds are shown on the *left* for Kv4.1 and on the *right* for Kv4.3. *A*, Summary for MS neurons. The Kv4.1 threshold distribution for MS neurons had a mode near one-quarter of the total single-cell cDNA. The distribution for Kv4.3 detection had a mode nearer one-half of the total cDNA. *B*, Summary for GP neurons. Note that Kv4.3 was present in high abundance in these neurons. *C*, Summary for basal forebrain cholinergic neurons. Kv4.1 was the most abundant in this population. *D*, Summary for neostriatal cholinergic interneurons. Note that Kv4.3 was present at low levels compared with that in GP neurons. *nd*, Not detected.

Kv4.3 mRNA abundance varied substantially (Fig. 6, *right*). In GP neurons, the modal detection threshold was near one-sixteenth of the total cDNA, whereas it was undetectable in 6 of 14 ChAT/str neurons, probably reflecting a very low Kv4.3 mRNA abundance in these cells. Kv4.3 transcripts were of intermediate abundance in MS neurons. In ChAT/bf cells, the Kv4.3 cDNA detection threshold was bimodal. This distribution may reflect the existence of two subpopulations, but no differences in current kinetics among ChAT/bf neurons were found. Kv4.3 transcripts were of intermediate abundance in MS and ChAT/bf neurons. Clearly, the abundance estimates for Kv4.1 and Kv4.3 transcripts were not correlated with A-type current amplitude.

#### Quantitative estimates of Kv4.2 mRNA abundance reveal a linear correlation with maximal A-type conductance

Because of the strong correlation between Kv4.2 mRNA abundance estimates and the amplitude of A-type currents, an attempt was made to quantify transcript levels in individual cells. The first step in this approach was to generate an external standard (Siebert and Larrick, 1992). To this end, a Kv4.2 cDNA fragment spanning the PCR amplification site was subcloned and harvested.



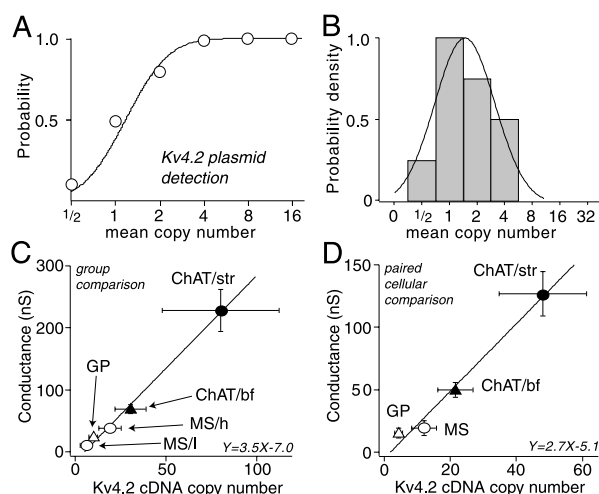


**Figure 7.** Maximum somatodendritic A-type conductance is directly correlated with estimates of Kv4.2 mRNA abundance. *A*, Plot of amplicon detection probability as a function of the number of plasmid DNA copies is shown. The solid line represents a fit of Gaussian cumulative function. *B*, Plot of probability density obtained from the data in *A* is shown. Each bar represents the normalized change in the probability of amplicon detection corresponding to the change in the mean copy number. *C*, Average maximal conductance is plotted against the mean estimated number of copies of Kv4.2 cDNA for each of the five cell groups. Copy number estimates were pooled for a group of neurons aspirated without recording as shown in Figure 5. MS neurons were split into high and low abundance groups (see Fig. 5*A*): MS/high (MS/h),  $n = 12$ , and MS/low (MS/l),  $n = 7$ . Conductance estimates were pooled for a group of neurons in which only phenotyping was done [GP neurons,  $n = 8$ ; ChAT/bf neurons,  $n = 9$ ; ChAT/str neurons,  $n = 6$ ; and MS neurons split into high and low conductance groups (see Fig. 5*A*), MS/high,  $n = 4$ , and MS/low,  $n = 5$ ]. The solid line shows the linear regression fit of data points; parameters are shown in the bottom right corner. *D*, In these experiments, recording and copy number estimates were made from the same cells (GP neurons,  $n = 6$ ; ChAT/bf neurons,  $n = 5$ ; ChAT/str neurons,  $n = 5$ ; and MS neurons,  $n = 7$ ). As in *C*, the linear regression is shown as a solid line. Note the similarity with *C*.

PCR calibration curves were generated by serially diluting a known concentration of Kv4.2 plasmid template and then performing PCR-based detection experiments as with individual neurons. Shown in Figure 7*A* is a plot of detection probability as a function of Kv4.2 plasmid copy number. The data were well fit with a Gaussian cumulative probability function. To generate estimates similar to those with the individual neurons, a threshold histogram was constructed as shown in Figure 7*B*. The threshold histogram was fit with a Gaussian density function, as with the individual neurons. The mode of the Gaussian function was 1.5 copies of single-stranded plasmid DNA. This provides an estimate of the modal number of Kv4.2 cDNAs in the detection experiments performed with the individual neurons. So, in ChAT/bf neurons, the mode of the detection histogram was one-twentieth of the total cDNA. That is, one-twentieth of the cellular cDNA must have contained, on average, 1.5 copies of Kv4.2 cDNA. This means that there were  $\sim 30$  (20 times 1.5) copies of Kv4.2 cDNA in the ChAT/bf neuron RT product. By the use of a similar argument, ChAT/str neurons yielded  $\sim 80$  copies of Kv4.2 cDNA. GP neurons were estimated to yield  $\sim 10$  Kv4.2 cDNA copies. MS neurons with high mRNA levels yielded  $\sim 20$  copies of Kv4.2 cDNA, whereas MS neurons with low abundance yielded 6 copies, on average.

To determine whether there was a quantitative relationship between mRNA abundance and channel number, the average

maximum A-type current conductance in each population was plotted as a function of mean Kv4.2 copy number (Fig. 7*C*). The maximum conductance was estimated by fitting the inactivating phase of the current evoked by a step to 0 mV and extrapolating back to the beginning of the voltage step. The conductance estimate should be within a multiplicative constant of the number of A-type channels in the somatodendritic membrane. To aid in the analysis, the MS population was broken into high and low Kv4.2 mRNA-expressing groups (as described above). Similarly, neurons exhibiting high and low A-type conductances were broken into two groups before averaging (see Fig. 5*A*, inset). The high degree of correlation between A-type conductance (channel) estimates and those of Kv4.2 copy number is readily apparent. A linear regression analysis confirmed the significance of the correlation ( $R^2 = 0.996$ ;  $p < 0.001$ ).

Although the variance in the grouped estimates was relatively small, an attempt was made to determine whether Kv4.2 copy number could be matched to conductance estimates in the same neuron. In these experiments, the cytoplasm was harvested after determining maximum A-type conductance. Serial dilution experiments were then performed to generate estimates of Kv4.2 cDNA abundance. The maximum conductance measurements are plotted against Kv4.2 cDNA estimates in four populations of neurons in Figure 7*D*. Because these measurements were paired, MS neurons were not broken into groups in this plot. The correlation seen here was similar to that found in the grouped data and highly significant ( $R^2 = 0.98$ ;  $p < 0.01$ ). Note that the regressions in Figure 7, *C* and *D*, had very similar slopes and intercepts near the origin, in spite of the variation in current amplitudes and estimated copy number.

An alternative method for generating quantitative estimates of transcript abundance is real-time PCR (Gibson et al., 1996; Heid et al., 1996). This approach uses fluorescent probes to estimate amplicon abundance as the PCR reaction proceeds. By monitoring the accumulation of PCR amplicon, PCR efficiency and progress can be monitored. Figure 8*A* shows single-cell Kv4.2 PCR amplification plots generated from ChAT/str and ChAT/bf neurons. Quantification of the initial transcript abundance relies on determining the cycle number at which the fluorescence signal crosses a predetermined threshold (defined as the mean background fluorescence plus 10 times the SD in cycles 3–15). The cycle number at which the detection threshold is crossed ( $C_T$ ) is proportional to the log of the initial transcript copy number (Heid et al., 1996). The amplification was calibrated using known copy numbers of plasmid Kv4.2 cDNA. The regression line fit to these data is shown in Figure 8*B*. Superimposed on the calibration line are the average  $C_T$  values for the sample of ChAT/str and ChAT/bf neurons. The corresponding values on the x-axis are estimates of the starting copy number in each group. In ChAT/bf neurons the estimated copy number was 5.2. Because one-fifth of the total cellular cDNA was used in the reaction, this translates to  $\sim 26 \pm 6$  (SEM) Kv4.2 cDNA copies per neuron. Similarly, in ChAT/str neurons the sample copy number was 12.4, which translates to  $\sim 62 \pm 5$  copies of Kv4.2 cDNA per neuron. These predictions were similar to those obtained with the serial dilution approach in which it was estimated that there were  $\sim 30$  Kv4.2 cDNA copies per ChAT/bf neuron and 80 Kv4.2 cDNA copies per ChAT/str neuron. Copy number estimates using this approach were not possible for GP and MS neurons for two reasons. First, including more than one-fifth of the cellular cDNA in the PCR reaction decreased amplification efficiency. Second, because of sensitivity limitations, calibration was unreliable at copy num-

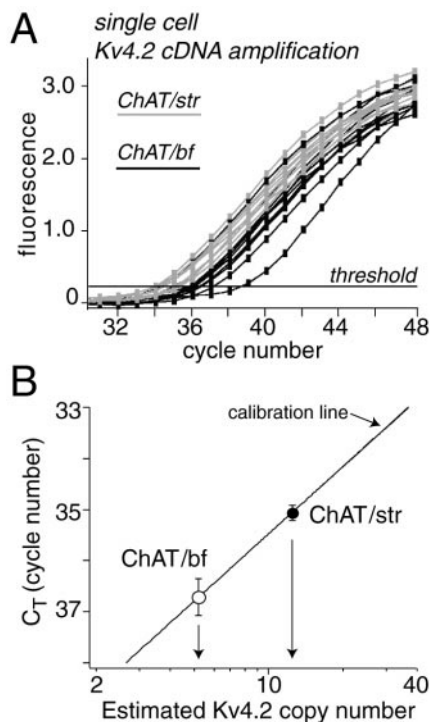


**Figure 8.** Kv4.2 cDNA quantification in ChAT neurons using fluorimetric detection. *A*, Plot of fluorescence as a function of PCR cycle number is shown. Two PCR reactions were performed for each cell. One-fifth of the total cellular cDNA was used for each reaction. Dark lines were generated from ChAT/bf neurons, whereas the lighter lines were generated from ChAT/str neurons. The horizontal line shows the fluorescence threshold.  $C_T$  is defined as a cycle number at which fluorescence crosses the threshold. *B*, The solid line is a calibration plot generated with known concentrations of plasmid Kv4.2 cDNA. Superimposed on the line are the mean ( $\pm$  SEM)  $C_T$  values for ChAT/bf ( $n = 5$ ) and ChAT/str ( $n = 4$ ) groups. Arrows indicate the estimated average number of Kv4.2 cDNA copies in one-fifth of the total cellular cDNA in these two cell groups.

bers less than  $\sim 5$ . Because both GP and MS neurons typically had  $<5$  Kv4.2 cDNA copies in aliquots containing one-fifth of the total cellular cDNA, accurate quantification by the fluorimetric method was not possible.

## DISCUSSION

### Kv4.2 subunits are major constituents of A-type $K^+$ channels in basal ganglia and basal forebrain neurons

In agreement with previous studies (Surmeier et al., 1989; Stefani et al., 1992; Sim and Allen, 1998; Song et al., 1998), A-type  $K^+$  currents were evident in three types of basal ganglia neuron and in basal forebrain cholinergic neurons. The pharmacological and biophysical features of the A-type current in these neurons were consistent with the hypothesis that they were attributable to Kv4 family channels (Baldwin et al., 1991; Pak et al., 1991; Roberds and Tamkun, 1991; Serodio et al., 1994, 1996). In particular, these currents (1) were sensitive to 4-AP but insensitive to TEA, (2) activated at hyperpolarized membrane potentials and inactivated rapidly, and (3) recovered from inactivation relatively rapidly without a prominent recovery time constant of several seconds. The latter feature distinguishes Kv4 family and homomeric Kv1.4 channels (Bertoli et al., 1994, 1996; Serodio et al., 1994; Petersen and Nerbonne, 1999). However, heteromeric channels containing Kv1.4 and Kv1.2 subunits have been reported to recover more rapidly (Po et al., 1993), making it impossible to exclude these

channels as contributors on the basis of these features alone. However, other observations are inconsistent with a dominant role for Kv1.4 subunits. In particular, the pronounced allosteric effects of  $Cd^{2+}$  on channel activation are typical of Kv4 but not Kv1 family channels (Wickenden et al., 1999). Also, immunocytochemical studies have localized Kv4 family subunits in the somatodendritic membrane and Kv1.4 subunits in axonal regions for the most part (Sheng et al., 1992; Maletic-Savatic et al., 1995; Rhodes et al., 1997; Cooper et al., 1998; Rasband et al., 1998; Song et al., 1998). Taken together, these observations are strongly suggestive of a major role for Kv4 family channels in the generation of A-type  $K^+$  currents in the somatodendritic membrane of the neurons studied here, but they are not conclusive.

An independent line of evidence that makes the case for this hypothesis considerably stronger comes from our scRT-PCR analysis. These studies showed that all three cloned members of this family—Kv4.1, Kv4.2, and Kv4.3—were expressed at readily detectable levels in all four neuron types. More importantly, the relative abundance of Kv4.2 mRNA was positively correlated with measures of maximum A-type conductance across this population. The relative abundance estimates used in this analysis relied on serial dilution scRT-PCR (Tkatch et al., 1998). Although not capable of determining absolute mRNA levels, this approach minimizes assumptions about reverse transcription and PCR efficiency in assuming that these parameters are the same for all cell types. The generation of more quantitative estimates required the introduction of a standard that could be used to calibrate reaction conditions. To this end, a fragment of the Kv4.2 transcript targeted by our PCR primers was subcloned. This standard was then used to estimate quantitatively Kv4.2 cDNA abundance in the material reverse transcribed from individual neurons. These studies yielded estimates that ranged from 6 Kv4.2 cDNA copies in one subpopulation of medium spiny neurons to 80 copies in striatal cholinergic interneurons. The Kv4.2 cDNA estimates in neostriatal cholinergic interneurons and basal forebrain cholinergic neurons were corroborated by fluorimetric quantitative PCR. Although not direct estimates of mRNA abundance, these measures of cDNA copy number should be proportional to actual mRNA numbers. To get at mRNA levels directly, reverse transcription efficiency for the Kv4.2 mRNA transcript would need to be determined. Because this parameter is likely to depend on mRNA secondary structure and protein/RNA binding, it is unlikely that anything less than a near full-length RNA standard that mimics the 3'-untranslated region will yield an accurate estimate. For the questions posed here, the investment in the construction of such a standard was not warranted.

The key question to be asked of these molecular data is whether the data were quantitatively related to the number of functional A-type channels. To generate an approximate estimate of channel number, extrapolated peak current measurements were taken at depolarized potentials at which open probability should be maximal (Baro et al., 1997). This measure should be directly proportional to the number of channels in the somatic and proximal dendritic membrane (Hille, 1992). This indirect estimate of A-type channel number exhibited a strikingly linear correlation with Kv4.2 cDNA abundance estimates derived from independent scRT-PCR-profiling experiments in which neurons were not recorded from to maximize mRNA recovery. This precaution (taken to avoid spurious mRNA degradation) turned out to be unnecessary, because a very similar relationship was found in neurons subjected to both recording and scRT-PCR analysis. A linear correlation also has been reported between



A-type current amplitude and Shal cDNA abundance in lobster pyloric neurons (Baro et al., 1997). In this case, the relationship between conductance and transcript number was  $\sim 1.25$  nS/transcript. In our case, the slope of the relationship was  $\sim 2$  nS/transcript. This is surprisingly close given the differences in species, cell sizes, preparations, and recording conditions.

The most parsimonious interpretation of these results is that the TEA-insensitive A-type channels in the somatodendritic membrane of these four neuron types are composed primarily of Kv4.2  $\alpha$  subunits. This conclusion is consistent with our previous studies of neostriatal cholinergic interneurons (Song et al., 1998). An important question that remains unanswered is the precise composition of these channels. Kv4  $\alpha$  subunits form subfamily-specific tetrameric channels; that is, they do not aggregate with  $\alpha$  subunits from other gene families (Xu et al., 1995), but they can form heteromultimers (Johns et al., 1997). It is unlikely, on the basis of our results, that the stoichiometric relationship between Kv4.2 and other Kv4 family subunits is fixed across neuronal populations. If it were, then the abundance of Kv4.1 or Kv4.3 transcripts would be correlated with current amplitudes, just as for Kv4.2 transcripts (which was not the case). Although the contribution of other Kv4 family subunits may vary from cell type to cell type, our results argue that the number of Kv4.2  $\alpha$  subunits per channel is the same in the four types of neurons studied. It is unclear what the functional consequences of this architectural feature are at this point, but given the biophysical similarity of channels arising from Kv4.1, Kv4.2, and Kv4.3 subunits, it is tempting to speculate that subunit composition influences other channel properties such as subcellular localization (Sheng et al., 1992; Klumpp et al., 1995; Maletic-Savatic et al., 1995; Alonso and Widmer, 1997) or ancillary subunit association (Serodio et al., 1994; Nakahira et al., 1996; Rhodes et al., 1997).

### Variation in gating properties suggests that determinants other than $\alpha$ subunits contribute to channel function

In spite of the apparent molecular similarities of the A-type channels in each of the neuronal populations studied, there were substantial differences in their gating properties. Significant differences were found in steady-state activation and inactivation voltage dependence. Significant differences were also found in the kinetics of inactivation development and recovery. Some of these properties covaried. For example, in those GP neurons in which the development of inactivation was slow, the recovery from inactivation also was relatively slow. In medium spiny neurons, the development of inactivation was relatively rapid, as was the recovery from inactivation. However, in other cases there were deviations from this simple pattern. For example, in neostriatal cholinergic interneurons the development of inactivation was fast and monoexponential, whereas the recovery from inactivation had both fast and slow components.

What are the origins of this heterogeneity in gating properties? It is unlikely that an explanation can be found in the differential expression of Kv4.1 and Kv4.3 mRNAs for at least two reasons. First, in heterologous expression systems, there are not marked differences in the gating properties of Kv4.1, Kv4.2, or Kv4.3 channels. Second, there was no correlation between the gating properties of A-type current and the expression levels of Kv4.1 or Kv4.3 mRNA across the cell types studied here. For example, the inactivation rate was clearly biexponential in GP and basal forebrain neurons but primarily monoexponential in medium spiny and cholinergic interneurons. Neither Kv4.1 nor Kv4.3 abundance

estimates covaried with this parameter. Attempts to correlate other biophysical properties with the expression levels of these other subunits also have proven fruitless.

If variation in the incorporation of the Kv4 family subunits does not explain the differences in gating properties, then what does? One possibility is that channel phosphorylation may be responsible. For example, serine/threonine kinase phosphorylation of Kv4 family channels can alter fast inactivation kinetics (Covarrubias et al., 1994; Nakamura et al., 1997) as well as steady-state voltage dependence (Akins et al., 1990; Hoffman and Johnston, 1998). Variation in membrane composition also can alter gating kinetics (Chang et al., 1995). Another intriguing possibility is that auxiliary subunits are responsible. There are several lines of evidence to support this proposition. The most direct of these is the demonstration that coexpression of small-molecular weight mRNA with Kv4.2 mRNA has significant effects on gating kinetics and voltage dependence (Serodio et al., 1994). Moreover, recent work has shown that the expression of Kv4.2 subunits in human embryonic kidney (HEK)-293 cells results in currents with a number of properties similar to those found in GP and basal forebrain cholinergic neurons and unlike those in *Xenopus* oocytes (Petersen and Nerbonne, 1999), suggesting that HEK-293 cells express an auxiliary subunit capable of regulating channel gating. Developmental regulation of subunit expression could account for age-related changes in the kinetics of A-type currents (Raucher and Dryer, 1994), as well as provide a powerful tool for tuning channel properties in individual cells.

Understanding the molecular basis for this variation in gating is crucial to any transgenic strategy (Johns et al., 1997) aimed at regularizing disordered spike patterning that can be traced to A-type channels. In parkinsonian primates and in human Parkinson's disease patients, for example, GP neurons begin to exhibit burst firing unlike that seen in normal tissue (Bergman et al., 1998). The importance of A-type currents in generating slow repetitive discharge (Connor and Stevens, 1971) suggests that a reduction in these currents could be a contributing factor in this pathophysiology. A functional downregulation could come as a consequence of reduced Kv4.2 subunit expression and/or stability or from an increased inactivation of Kv4.2 channels attributable to alteration in these other determinants.

### REFERENCES

- Akins PT, Surmeier DJ, Kitai ST (1990) Muscarinic modulation of the transient potassium current in rat neostriatal neurons. *Nature* 344:240–242.
- Alonso G, Widmer H (1997) Clustering of KV4.2 potassium channels in postsynaptic membrane of rat supraoptic neurons: an ultrastructural study. *Neuroscience* 77:617–621.
- Audinat E, Lambolez B, Rossier J (1996) Functional and molecular analysis of glutamate-gated channels by patch-clamp and RT-PCR at the single cell level. *Neurochem Int* 28:119–136.
- Baldwin TJ, Tsaur ML, Lopez GA, Jan YN, Jan LY (1991) Characterization of a mammalian cDNA for an inactivating voltage-sensitive K<sup>+</sup> channel. *Neuron* 7:471–483.
- Baro DJ, Levini RM, Kim MT, Willms AR, Lanning CC, Rodriguez HE, Harris-Warrick RM (1997) Quantitative single-cell-reverse transcription-PCR demonstrates that A-current magnitude varies as a linear function of shal gene expression in identified stomatogastric neurons. *J Neurosci* 17:6597–6610.
- Bergman H, Feingold A, Nini A, Raz A, Slovlin H, Abeles M, Vaadia E (1998) Physiological aspects of information processing in the basal ganglia of normal and parkinsonian primates. *Trends Neurosci* 21:32–38.
- Bertoli A, Moran O, Conti F (1994) Activation and deactivation properties of rat brain K<sup>+</sup> channels of the Shaker-related subfamily. *Eur Biophys J* 23:379–384.

- Bertoli A, Moran O, Conti F (1996) Accumulation of long-lasting inactivation in rat brain K(+) channels. *Exp Brain Res* 110:401–412.
- Chang HM, Reitsstetter R, Gruener R (1995) Lipid-ion channel interactions: increasing phospholipid headgroup size but not ordering acyl chains alters reconstituted channel behavior. *J Membr Biol* 145:13–19.
- Cimino GD, Metchetti K, Isaacs ST, Zhu YS (1990) More false-positive problems. *Nature* 345:773–774.
- Connor JA, Stevens CF (1971) Voltage clamp studies of a transient outward membrane current in gastropod neural somata. *J Physiol (Lond)* 213:21–30.
- Cooper EC, Milroy A, Jan YN, Jan LY, Lowenstein DH (1998) Presynaptic localization of Kv1.4-containing A-type potassium channels near excitatory synapses in the hippocampus. *J Neurosci* 18:965–974.
- Covarrubias M, Wei A, Salkoff L, Vyas TB (1994) Elimination of rapid potassium channel inactivation by phosphorylation of the inactivation gate. *Neuron* 13:1403–1412.
- Dryer L, Xu Z, Dryer SE (1998) Arachidonic acid-sensitive A-currents and multiple Kv4 transcripts are expressed in chick ciliary ganglion neurons. *Brain Res* 789:162–166.
- Fiset C, Clark RB, Shimoni Y, Giles WR (1997) Shal-type channels contribute to the Ca<sup>2+</sup>-independent transient outward K<sup>+</sup> current in rat ventricle. *J Physiol (Lond)* 500:51–64.
- Gibson UE, Heid CA, Williams PM (1996) A novel method for real time quantitative RT-PCR. *Genome Res* 6:995–1001.
- Hagiwara S, Kusano K, Saito N (1961) Membrane changes of *Onchidium* nerve cells in potassium rich media. *J Physiol (Lond)* 155:470–489.
- Hamill OP, Marty A, Neher E, Sakmann B, Sigworth FJ (1981) Improved patch-clamp techniques for high resolution current recording from cells and cell-free membrane patches. *Pflügers Arch* 391:85–100.
- Heid CA, Stevens J, Livak KJ, Williams PM (1996) Real time quantitative PCR. *Genome Res* 6:986–994.
- Heinemann SH, Rettig J, Graack HR, Pongs O (1996) Functional characterization of Kv channel beta-subunits from rat brain. *J Physiol (Lond)* 493:625–633.
- Hille B (1992) Ionic channels of excitable membranes. Sunderland, MA: Sinauer.
- Hoffman DA, Johnston D (1998) Downregulation of transient K<sup>+</sup> channels in dendrites of hippocampal CA1 pyramidal neurons by activation of PKA and PKC. *J Neurosci* 18:3521–3528.
- Johns DC, Nuss HB, Marban E (1997) Suppression of neuronal and cardiac transient outward currents by viral gene transfer of dominant-negative Kv4.2 constructs. *J Biol Chem* 272:31598–31603.
- Kanold PO, Manis PB (1999) Transient potassium currents regulate the discharge patterns of dorsal cochlear nucleus pyramidal cells. *J Neurosci* 19:2195–2208.
- Klumpp DJ, Song EJ, Pinto LH (1995) Identification and localization of K<sup>+</sup> channels in the mouse retina. *Vis Neurosci* 12:1177–1190.
- Maletic-Savatic M, Lenn NJ, Trimmer JS (1995) Differential spatiotemporal expression of K<sup>+</sup> channel polypeptides in rat hippocampal neurons developing *in situ* and *in vitro*. *J Neurosci* 15:3840–3851.
- Martina M, Schultz JH, Ehmke H, Monyer H, Jonas P (1998) Functional and molecular differences between voltage-gated K<sup>+</sup> channels of fast-spiking interneurons and pyramidal neurons of rat hippocampus. *J Neurosci* 18:8111–8125.
- Nakahira K, Shi G, Rhodes KJ, Trimmer JS (1996) Selective interaction of voltage-gated K<sup>+</sup> channel beta-subunits with alpha-subunits. *J Biol Chem* 271:7084–7089.
- Nakamura TY, Coetzee WA, Vega-Saenz De Miera E, Artman M, Rudy B (1997) Modulation of Kv4 channels, key components of rat ventricular transient outward K<sup>+</sup> current, by PKC. *Am J Physiol* 273:H1775–H1786.
- Pak MD, Baker K, Covarrubias M, Butler A, Ratcliffe A, Salkoff L (1991) mShal, a subfamily of A-type K<sup>+</sup> channel cloned from mammalian brain. *Proc Natl Acad Sci USA* 88:4386–4390.
- Petersen KR, Nerbonne JM (1999) Expression environment determines K<sup>+</sup> current properties: Kv1 and Kv4 alpha-subunit-induced K<sup>+</sup> currents in mammalian cell lines and cardiac myocytes. *Pflügers Arch* 437:381–392.
- Po S, Roberds S, Snyders DJ, Tamkun MM, Bennett PB (1993) Heteromultimeric assembly of human potassium channels. Molecular basis of a transient outward current? *Circ Res* 72:1326–1336.
- Rasband MN, Trimmer JS, Schwarz TL, Levinson SR, Ellisman MH, Schachner M, Shrager P (1998) Potassium channel distribution, clustering, and function in remyelinating rat axons. *J Neurosci* 18:36–47.
- Raucher S, Dryer SE (1994) Functional expression of A-currents in embryonic chick sympathetic neurones during development *in situ* and *in vitro*. *J Physiol (Lond)* 479:77–93.
- Rettig J, Heinemann SH, Wunder F, Lorra C, Parcej DN, Dolly JO, Pongs O (1994) Inactivation properties of voltage-gated K<sup>+</sup> channels altered by presence of beta-subunit. *Nature* 369:289–294.
- Rhodes KJ, Strassle BW, Monaghan MM, Bekele-Arcuri Z, Matos MF, Trimmer JS (1997) Association and colocalization of the Kvbeta1 and Kvbeta2 beta-subunits with Kv1 alpha-subunits in mammalian brain K<sup>+</sup> channel complexes. *J Neurosci* 17:8246–8258.
- Roberds SL, Tamkun MM (1991) Cloning and tissue-specific expression of five voltage-gated potassium channel cDNAs expressed in rat heart. *Proc Natl Acad Sci USA* 88:1798–1802.
- Rudy B (1988) Diversity and ubiquity of K channels. *Neuroscience* 25:729–749.
- Schroter KH, Ruppersberg JP, Wunder F, Rettig J, Stocker M, Pongs O (1991) Cloning and functional expression of a TEA-sensitive A-type potassium channel from rat brain. *FEBS Lett* 278:211–216.
- Serodio P, Kentros C, Rudy B (1994) Identification of molecular components of A-type channels activating at subthreshold potentials. *J Neurophysiol* 72:1516–1529.
- Serodio P, Vega-Saenz de Miera E, Rudy B (1996) Cloning of a novel component of A-type K<sup>+</sup> channels operating at subthreshold potentials with unique expression in heart and brain. *J Neurophysiol* 75:2174–2179.
- Sheng M, Tsaur ML, Jan YN, Jan LY (1992) Subcellular segregation of two A-type K<sup>+</sup> channel proteins in rat central neurons. *Neuron* 9:271–284.
- Shi W, Wymore RS, Wang HS, Pan Z, Cohen IS, McKinnon D, Dixon JE (1997) Identification of two nervous system-specific members of the erg potassium channel gene family. *J Neurosci* 17:9423–9432.
- Siebert PD, Larrick JW (1992) Competitive PCR. *Nature* 359:557–558.
- Sim JA, Allen TG (1998) Morphological and membrane properties of rat magnocellular basal forebrain neurons maintained in culture. *J Neurophysiol* 80:1653–1669.
- Song W-J, Surmeier DJ (1996) Voltage-dependent facilitation of calcium currents in rat neostriatal neurons. *J Neurophysiol* 76:2290–2306.
- Song WJ, Tkatch T, Baranauskas G, Ichinohe N, Kitai ST, Surmeier DJ (1998) Somatodendritic depolarization-activated potassium currents in rat neostriatal cholinergic interneurons are predominantly of the A type and attributable to coexpression of Kv4.2 and Kv4.1 subunits. *J Neurosci* 18:3124–3137.
- Stefani A, Calabresi P, Mercuri NB, Bernardi G (1992) A-current in rat globus pallidus: a whole-cell voltage clamp study on acutely dissociated neurons. *Neurosci Lett* 144:4–8.
- Stuhmer W, Ruppersberg JP, Schroter KH, Sakmann B, Stocker M, Giese KP, Perschke A, Baumann A, Pongs O (1989) Molecular basis of functional diversity of voltage-gated potassium channels in mammalian brain. *EMBO J* 8:3235–3244.
- Surmeier DJ, Bargas J, Kitai ST (1989) Two types of A-current differing in voltage-dependence are expressed by neurons of the rat neostriatum. *Neurosci Lett* 103:331–337.
- Surmeier DJ, Bargas J, Hemmings Jr HC, Nairn AC, Greengard P (1995) Modulation of calcium currents by a D1 dopaminergic protein kinase/phosphatase cascade in rat neostriatal neurons. *Neuron* 14:385–397.
- Surmeier DJ, Song WJ, Yan Z (1996) Coordinated expression of dopamine receptors in neostriatal medium spiny neurons. *J Neurosci* 16:6579–6591.
- Sykes PJ, Neoh SH, Brisco MJ, Hughes E, Condon J, Morley AA (1992) Quantitation of targets for PCR by use of limiting dilution. *Biotechniques* 13:444–449.
- Tkatch T, Baranauskas G, Surmeier DJ (1998) Basal forebrain neurons adjacent to the globus pallidus co-express GABAergic and cholinergic marker mRNAs. *NeuroReport* 9:1935–1939.
- Wickenden AD, Tsushima RG, Losito VA, Kaprielian R, Backx PH (1999) Effect of Cd<sup>2+</sup> on Kv4.2 and Kv1.4 expressed in *Xenopus* oocytes and on the transient outward currents in rat and rabbit ventricular myocytes. *Cell Physiol Biochem* 9:11–28.
- Xu J, Yu W, Jan YN, Jan LY, Li M (1995) Assembly of voltage-gated potassium channels. Conserved hydrophilic motifs determine subfamily-specific interactions between the alpha-subunits. *J Biol Chem* 270:24761–24768.
- Yan Z, Surmeier DJ (1996) Muscarinic (m2/m4) receptors reduce N- and P-type Ca<sup>2+</sup> currents in rat neostriatal cholinergic interneurons through a fast, membrane-delimited, G-protein pathway. *J Neurosci* 16:2592–2604.